Pergamon

International Journal of Plasticity, Vol. 11, No. 4, pp. 471–499, 1995

0749-6419/95 $9.50 + .00

0749-6419(95)00009-7

# A MACROSCOPIC MODEL FOR PLASTIC FLOW IN METAL-MATRIX COMPOSITES

HONG-TAO ZHU and HUSSEIN M. ZBIB

Washington State University

(Communicated by George Weng, Rutgers University)

**Abstract**—A micromechanically based continuum model is developed to analyze the enhancement of plastic properties of particulate-reinforced metal-matrix composites over matrix materials. The composite is idealized as uniformly distributed periodic arrays of unit cells. Each unit cell consists of a rigid inclusion surrounded by a plastically deforming material. An energy method is adopted to obtain the overall constitutive relation for the composite on the basis of the local nonuniform deformation fields. Effects of particle volume fractions and shapes (e.g. whiskers, discs, etc.) as well as the matrix properties on the flow properties of the composite are obtained. The results are in good agreement with experimental observations and finite element analyses found in the literature. An explicit expression is also proposed, providing a means for evaluating various factors affecting the strength of composites.

## I. INTRODUCTION

Generally, two-phase composite materials have certain advanced and improved thermomechanical properties that make them more attractive to use in the production of major components in various industries, such as automobile and aircraft. In particular, aluminum alloys reinforced with relatively rigid particles that do not deform plastically, such as SiC particles and alumina particles, have properties that make them very attractive for consideration over other metal-matrix composites that have directional structures. Although discontinuous particulate-reinforced metal matrix composites (MMCs) do not have the very high directional strength of continuously fiber-reinforced composites, their isotropic properties retain some of the traditional fabricability and formability of aluminum alloys, making them potentially more economical to produce. Due to the isotropic nature of these composites, their overall mechanical properties are very much determined by those of the matrix and the volume, size, and spacings of the rigid particles. Optimization of the flow and strength properties of such composites hinges on our knowledge of the fundamental relationships between the macroscopic behavior of the composites and its microstructure. Particle dimensions, their distribution and density are some of the basic microstructural features that have significant influence on the mechanical macroscopic response of the MMCs.

Experimental characterization of the mechanical properties of MMCs has been conducted by a number of investigators; we mention, for example, the recent works of PAPAZIAN and ADLER [1990], KAMAT *et al.* [1991], and EVANS *et al.* [1991]. A more detailed review of the subject can be found in the VIEWPOINT SET [1991]. In these works the composite is tested for its strength for different particle densities. For example, the

work of PAPAZIAN and ADLER [1990] presents results pertaining to Al alloys reinforced with SiC particles. It is shown that the addition of these particles increases the elastic modulus, the overall yield stress, and the work hardening rate, but the strain to failure decreases. Most of these works examined large particle sizes in the range of micrometers, where it is generally considered that continuum models apply, and predicted that the yield stress was a function of the volume fraction of the particles. However, a recent study by KAMAT *et al.* [1991] on composites comprising alumina particulate in either 2014O or 2024O aluminum alloy matrices indicates that the yield stress and work-hardening are very much affected by the size and spacing of the particles, in addition to the volume fraction, even in the micrometer range.

It seems that, although many aspects of MMCs are well explained, understanding of the strengthening mechanisms is still a subject that needs further investigation. For smaller particle sizes the dislocation-crystal plasticity description seems to give a good explanation of the mechanism. For example, the Orowan dislocation model (BROWN [1980]) for point-like pinning (small particles) predicts that the yield stress would vary with the inverse of the particle spacing. The present work studies the constitutive behavior of MMCs with large particle sizes and proposes the use of a micromechanical model, consisting of a finite unit cell and an embedded inclusion. The objective is to investigate the flow strength of MMCs and to rigorously derive the flow strength of composites composed of a power-law plastic material with rigid inclusions.

A closely related problem was examined by BUDIANSKY *et al.* [1982] (see also DUVA & HUTCHINSON [1984]) who considered the deformation of an infinite solid containing a void. In this approach an upper bound solution was obtained where approximate velocity fields were assumed by the superposition of a uniform field due to a uniform remote axisymmetric stress in the absence of the void, and an additional nonuniform one. Then a Rayleigh–Ritz method based on the minimum principle was used to generate approximate solutions in the material. DUVA [1984] used a similar method to analyze the stiffening effect of rigid inclusions on an infinite domain of a power-law material. Based on the potential function approach, a self-consistent differential equation was derived whose solution yielded the hardening of the composites. Since interactions between neighboring inclusions were ignored, the validity of the equation was limited to small concentrations of inclusions. Recently the calculation has been generalized by LEE and MEAR [1991,1992] for composites with elliptical or ellipsoidal inclusions to examine the effect of inclusion shape on the strength of composites. They first solved a kernel problem for an isolated inclusion in an infinite block and obtained constitutive relations for dilute inclusion concentrations. Then a differential self-consistent scheme was employed for the extensions to nondilute concentrations. Other theoretical approaches in this field include the modification of the method of MORI and TANAKA [1973] (see, for example, ZHAO & WENG [1990] and QIU & WENG [1991]), and the use of variational procedure (see PONTE CASTANEDA [1991] and LI & PONTE CASTANEDA [1993]).

We point out that the theory of composites of linear elastic materials is very well developed, and methods based on the use of Eshelby's solution of a single inclusion embedded in an infinite matrix have been developed and employed by many investigators (for example, the self-consistent method and the Mori–Tanaka method; HILL [1965] and WENG [1984]), where the rule of mixture is also used to relate the average stress or strain quantities to their local values. In this work we focus our attention on nonlinear viscoplastic materials and derive the overall macroscopic response of the composite through a volume averaging procedure as discussed below.

Since the complexity of the microstructural geometry of particle reinforced MMCs makes theoretical modelling rather difficult, many analyses are based on finite element

methods. TVERGAARD [1990] analyzed the tensile properties of a ductile metal reinforced by a periodic arrays of short fibers assuming that the whisker ends are not perfectly aligned but staggered (see also LEVY & PAPAZIAN [1990]). The results for rigid and elastic fibers show that the difference lies in the initial elastic range and the overall stress–strain behavior is dominated by the matrix plasticity. In the study of CHRISTMAN *et al.* [1989a] several models of uniformly distributed and nonuniformly distributed (clustering) particles, which are spherical or cylindrical in shape, were examined. Their results demonstrated that particle clustering causes a reduction in the yield strength of the composites.

The work of BAO *et al.* [1991] combined the finite element methods with the theoretical investigation. Their theoretical models were characterized by elastic–perfectly plastic behavior and power-law hardening behavior of the Ramberg–Osgood type. They used the finite element analysis to approximate the parameters in the models, which can reflect the effect of volume fraction and particle shape. In most of these analyses, an axisymmetric unit cell was assumed in the finite element calculations.

The purpose of the present work is to develop a mathematical model capable of capturing the basic features of plastic properties of the MMCs. The main goals are to rigorously derive the relationship that describes the overall nonlinear plastic response of the composite and to understand how the underlying microstructural variables influence the macroscopic properties. Unlike other models, dealing with an isolated inclusion in an unbounded medium (e.g. DUVA [1984] and LEE & MEAR [1991]), this work is based on the use of a finite unit cell accounting for the interaction of particles in composites with periodic microstructures. A minimum principle for the velocity field is adopted, yielding an upper bound solution for the flow strength of the composite. This method is motivated by the work of GURSON [1977] on yield surfaces for porous materials.

In Section II, the general approach is discussed, which employs an energy method to obtain the upper bound flow stress of the composite. Section III contains the results for a power-law viscoplastic matrix. Effects of particle volume fraction and particle shapes as well as the matrix properties on the flow strength of MMC are obtained. In Section IV, the results are discussed and compared with experimental observations and other models found in the literature. Finally, a model for the flow strength of MMC is proposed which captures the effect of particle density and shape as well as the matrix properties on the overall behavior of the composite, providing a means for evaluating various compositions.

## II. THEORETICAL FRAMEWORK

### II.1. *General approach*

In general, an arbitrary distribution of particles, which may include local clustering, may better represent the actual state of the composite. This, however, will complicate the problem and make it difficult if not impossible to proceed with an analytical approach. Thus, in this article we consider an idealized situation in which the particles are assumed to be uniformly distributed in the matrix in the form of periodic arrays. (Effect of clustering and nonperiodicity will be examined in a future article within a nonlocal continuum mechanics approach.) This geometric arrangement allows us to consider a unit cell containing one inclusion. It is assumed that the shape of the unit cell is similar to that of the inclusion, simplifying further the complexity of the problem. This unit cell represents the basic block that we will analyze to evaluate the overall mechanical strength of the composite. The main objective is to relate the macroscopic

properties of the composite to those of the matrix and the microstructural variables describing the particle geometry. This is accomplished by a volume averaging procedure in which the macroscopic quantities, such as the stress tensor, **S**, and the strain rate tensor, **D**, are obtained by the volume average of their microscopic counterparts, which are indicated by $\boldsymbol{\sigma}$ and $\dot{\boldsymbol{\epsilon}}$.

The matrix is characterized as a ductile, incompressible, viscoplastic material obeying the power law hardening relation

$$\bar{\sigma} = \sigma_0 \left( \frac{\dot{\bar{\epsilon}}}{\dot{\epsilon}_0} \right)^m, \tag{1}$$

and the von Mises flow rule

$$\dot{\boldsymbol{\epsilon}} = \frac{3}{2} \frac{\dot{\bar{\epsilon}}}{\bar{\sigma}} \boldsymbol{\sigma}', \tag{2}$$

where $\sigma_0$ is the reference stress, $\dot{\epsilon}_0$ is the reference strain rate, $m$ is the strain rate sensitivity parameter, $\dot{\bar{\epsilon}} = (2\dot{\boldsymbol{\epsilon}} \cdot \dot{\boldsymbol{\epsilon}}/3)^{1/2}$ is the effective strain rate, $\bar{\sigma} = (3\boldsymbol{\sigma}' \cdot \boldsymbol{\sigma}'/2)^{1/2}$ is the effective stress, $\boldsymbol{\sigma}'$ is the deviatoric part of the microscopic Cauchy stress tensor $\boldsymbol{\sigma}$, and $\dot{\boldsymbol{\epsilon}}$ is the microscopic strain rate tensor defined by the symmetric part of the microscopic velocity (**v**) gradient as

$$\dot{\boldsymbol{\epsilon}} = \tfrac{1}{2}(\nabla \mathbf{v} + \nabla \mathbf{v}^T), \tag{3}$$

where $\nabla$ indicates the gradient operator with respect to the position vector **x**.

The approach seeks an upper bound solution in which a kinematically admissible microscopic velocity field in the unit cell is assumed. A general velocity field can be constructed from an infinite number of fields $\mathbf{v}_i(\mathbf{x})$ (see, for example, BISHOP & HILL [1951] and BUDIANSKY *et al.* [1982]) that satisfy incompressibility. Formally, one can write

$$\mathbf{v} = \sum_{i=1}^{\infty} c_i \mathbf{v}_i(\mathbf{x}), \tag{4}$$

where $c_i$s are arbitrary constants.

For the current problem, we assume a rigid particle with perfect bonding at the particle–matrix interface, such that the inner boundary condition for the velocity field in the matrix, with respect to a reference frame fixed at a point on the particle, is given by

$$\mathbf{v} = \mathbf{0} \quad \text{at inner boundary.} \tag{5}$$

The boundary condition at the outer surface of the unit cell links the macroscopic values of the strain rate tensor to the microscopic velocity field **v** through the compatibility requirement

$$\mathbf{v} = \mathbf{D} \cdot \mathbf{x} \quad \text{at outer boundary.} \tag{6}$$

where **D** is defined as the volume average of $\dot{\boldsymbol{\epsilon}}$, such that

$$\mathbf{D} = \frac{1}{V} \int_V \dot{\boldsymbol{\epsilon}} \, dV. \tag{7}$$

Among all velocity fields that meet the incompressibility and boundary conditions, the actual one should minimize the total rate of plastic dissipation (a degenerate of Hill's functional since the variation in the velocity field at the boundary is zero)

$$\dot{W} = \frac{1}{V}\int_V \boldsymbol{\sigma}\cdot\dot{\boldsymbol{\epsilon}}\, dV, \tag{8}$$

such that

$$\frac{\partial \dot{W}}{\partial c_i} = 0, \quad i = 1,2,3,\ldots \tag{9}$$

subject to the boundary conditions. Furthermore, the macroscopic stress tensor **S** can be obtained as the work conjugate of **D** by the equivalence of rate of plastic work

$$\dot{W} = \mathbf{S}\cdot\mathbf{D}. \tag{10}$$

For power law viscoplastic materials, with $\dot{W}$ being homogeneous in **D** and of a degree $m+1$ (i.e. $\dot{W}(k\mathbf{D}) = k^{m+1}\dot{W}(\mathbf{D})$), the stress tensor, **S**, is given by

$$\mathbf{S} = \frac{1}{m+1}\frac{\partial \dot{W}}{\partial \mathbf{D}}. \tag{11}$$

A detailed derivation is given in Section III.

## II.2. *Unit cells*

We consider two families of unit cells having the shapes of ellipsoids of revolution, which represent a wide range of inclusion shapes, ranging from whiskers to discs. One family is the prolate ellipsoids that extends vertically into whiskers (see Fig. 1a). The other is the oblate ellipsoids that extends horizontally into disc shapes (see Fig. 1b).

Let $(z^1,z^2,z^3) = (x,y,z)$ be the Cartesian coordinate system with the origin located at the ellipsoid center and the $z^3$-axis coincided with the axis of revolution, as shown in Fig. 1. The ellipsoidal coordinates $(x^1,x^2,x^3) \equiv (\alpha,\theta,\phi)$ are defined by the following transformation to the Cartesian coordinates (keeping $\eta$ constant)

$$\begin{aligned} z^1 &= (\sinh\eta)\alpha\sin\theta\cos\phi,\\ z^2 &= (\sinh\eta)\alpha\sin\theta\sin\phi,\\ z^3 &= (\cosh\eta)\alpha\cos\theta, \end{aligned} \tag{12}$$

for prolate ellipsoids, and

$$\begin{aligned} z^1 &= (\cosh\eta)\alpha\sin\theta\cos\phi,\\ z^2 &= (\cosh\eta)\alpha\sin\theta\sin\phi,\\ z^3 &= (\sinh\eta)\alpha\cos\theta, \end{aligned} \tag{13}$$

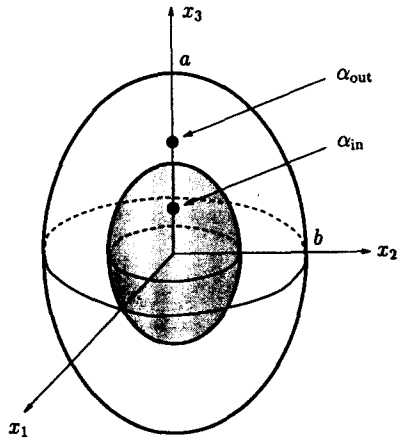


(a)

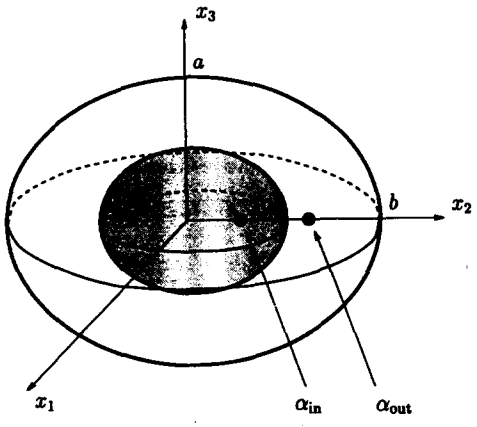


(b)

Fig. 1. Schematic diagrams of unit cells. (a) Prolate ellipsoidal cell. (b) Oblate ellipsoidal cell.

for oblate ellipsoids. In eqn (12) $\alpha$ is the focus distance of the ellipsoid and the parameter $\eta$ is related to the aspect ratio of the inclusion $K$, defined as

$$K = \frac{a}{b}, \tag{14}$$

by

$$K = \begin{cases} \dfrac{1}{\tanh \eta}, & \text{for prolate inclusions,} \\ \tanh \eta, & \text{for oblate inclusions,} \end{cases} \tag{15}$$

or

$$\eta = \begin{cases} \frac{1}{2} \ln \frac{K+1}{K-1}, & \text{for prolate inclusions,} \\ \frac{1}{2} \ln \frac{1+K}{1-K}, & \text{for oblate inclusions,} \end{cases} \tag{16}$$

The parameters $a$ and $b$ in eqn (14) are the inclusion half-height and the radius of revolution, respectively. For prolate inclusions, the aspect ratio $K$ is always greater than one and a large $K$ corresponds to a slender whisker. For oblate inclusions, $K$ is less than one and a thin disc has a small value of $K$. In both cases, $K \to 1$ represents spherical inclusions.

In this coordinate system, different values of $\alpha$ produce a family of parallel ellipsoids with different sizes but with the same shape factor $K$. Denoting the particle–matrix interface by $\alpha_1$ and the outer cell surface by $\alpha_2$, the particle volume fraction $f$ can be calculated by

$$f = \left(\frac{\alpha_1}{\alpha_2}\right)^3 \tag{17}$$

for both prolate and oblate inclusions.

We remark that the ellipsoidal coordinate system $(\alpha, \theta, \phi)$ defined by eqns (12) and (13) is different from the conventional one (i.e. the $(\eta, \theta, \phi)$ system, see MOON & SPENCER [1971] and LEE & MEAR [1991]) which represents a family of ellipsoids with the same focal distance but different aspect ratios. Although the currently used system $(\alpha, \theta, \phi)$ has the geometric properties we need, unfortunately, it is nonorthogonal, which leads to more complicated evaluations of velocity and strain fields.

For plastically incompressible matrix materials under axisymmetric loading conditions, a simple way to derive the physical components of the velocity vector $\mathbf{v}$ is to employ a stream function $\zeta$ such that $\mathbf{v} = \nabla \times (0, 0, \zeta)$ (see, for example, LEE & MEAR [1992]), yielding

$$\begin{aligned} v_\alpha &= \sqrt{\frac{g_{11}}{g}} \frac{\partial \zeta}{\partial \theta}, \\ v_\theta &= -\sqrt{\frac{g_{22}}{g}} \frac{\partial \zeta}{\partial \alpha}, \\ v_\phi &= 0, \end{aligned} \tag{18}$$

where $g_{11}, g_{22}$ are the covariant components and $g$ is the determinant of the metric tensor of the ellipsoidal coordinate systems. These quantities and other important geometric properties are all given in the Appendix for both prolate and oblate systems.

As for the choice of the stream function $\zeta(\alpha, \theta)$, a general form for a spherical model was given by BUDIANSKY *et al.* [1982] as

$$\zeta(r, \theta) = A \cot \theta + \sum_{k=2,4,\ldots} P_{k,\theta}(\cos \theta) f_k(r). \tag{19}$$

where $P_k$ is the Legendre polynomial of degree $k$, $f_k$ is a function of radius $r$ alone, and $A$ corresponds to the volume change. In this work, the following equivalent form of $\zeta$ is adopted

$$\zeta(\alpha,\theta) = -\frac{\sqrt{g}}{2\alpha^2} \sum_{k=2,4,\ldots} \sum_{i=-\infty}^{\infty} c_{ki}\alpha^i \sin k\theta, \tag{20}$$

where $k$, as in eqn (19), is taken to be even to represent the symmetric property of the velocity field with respect to the $x^3$-axis. The coefficient set $\{c_{ki}\}$ will be determined by minimizing the dissipation energy $\dot{W}$, subject to the constraints of the boundary conditions (5) and (6). In eqn (20) the term $-\sqrt{g}/(2\alpha^2)$ is chosen for convenience to match the boundary conditions.

We now derive an explicit form for the boundary conditions. The velocity field derived by (20) is

$$\begin{aligned} v_\alpha &= -\frac{\sqrt{g_{11}}}{2\alpha^2} \sum_{k=2,4,\ldots} \sum_{i=-\infty}^{\infty} c_{ki}\alpha^i(\cot\theta \sin k\theta + k\cos k\theta), \\ v_\theta &= -\frac{\sqrt{g_{22}}}{2\alpha^2} \sum_{k=2,4,\ldots} \sum_{i=-\infty}^{\infty} ic_{ki}\alpha^{i-1} \sin k\theta, \\ v_\phi &= 0. \end{aligned} \tag{21}$$

Expanding eqn (6) in ellipsoidal coordinates and noting that the macroscopic strain rate $\mathbf{D}$ has only principal values $D_{11} = D_{22}$ and $D_{33}$, we obtain the outer boundary conditions:

$$\begin{aligned} v_\alpha &= -\sqrt{g_{11}}D'\frac{\alpha}{6}(1 + 3\cos 2\theta), \quad \text{at } \alpha = \alpha_2, \\ v_\theta &= \sqrt{g_{22}}D'\tfrac{1}{2}\sin 2\theta; \\ D' &\equiv \frac{D_{11} + D_{22}}{2} - D_{33}. \end{aligned} \tag{22}$$

for both prolate and oblate systems.

Upon applying the boundary conditions (22) to the general solution (21) we obtain

$$\sum_{i=-\infty}^{\infty} c_{2i}\alpha_2^i = \frac{D'}{3}\alpha_2^3, \tag{23}$$

$$\sum_{i=-\infty}^{\infty} ic_{2i}\alpha_2^{i-1} = D'\alpha_2^2, \tag{24}$$

$$\sum_{i=-\infty}^{\infty} c_{ki}\alpha_2^i = \sum_{i=-\infty}^{\infty} ic_{ki}\alpha_2^{i-1} = 0, \quad k = 4,6,8,\ldots. \tag{25}$$

Eqns (23) and (24) arise from the first harmonic $\sin 2\theta$, which are necessary to identically satisfy the boundary conditions (18), while (25) arises from higher order harmonics ($\sin 4\theta, \sin 6\theta, \ldots$). According to BUDIANSKY *et al.* [1982] higher order harmonics have minor quantitative influence on the solution which involves volume averaging. (See also DUVA [1984] who uses only the lowest two harmonics.) Therefore, while identically satisfying the boundary conditions, one may drop these higher order harmonics by setting $c_{ki} = 0$, $k = 4,6,\ldots$ and reduce the computational effort. This is also adopted by GURSON [1977], who uses only the first harmonic in solving the void-matrix problem to ensure that the boundary conditions for the finite domain problem is identically met.

The inner boundary condition (5) can be written as

$$\sum_{i=-\infty}^{\infty} c_{2i}\alpha_1^i = 0,$$
$$\sum_{i=-\infty}^{\infty} ic_{2i}\alpha_1^{i-1} = 0. \tag{26}$$

By defining the following nondimensional quantities

$$B_i = \alpha_2^{i-3}c_{2i}, \qquad \lambda = \frac{\alpha}{\alpha_2}, \qquad \gamma = \frac{\alpha_1}{\alpha_2}, \tag{27}$$

the physical components of the velocity vector can then be written as

$$v_\alpha = -\frac{1}{2}\sqrt{g_{11}}(1 + 3\cos 2\theta)\alpha_2 \sum_{i=-\infty}^{\infty} B_i\lambda^{i-2},$$
$$v_\theta = \frac{1}{2}\sqrt{g_{22}}\sin 2\theta \sum_{i=-\infty}^{\infty} iB_i\lambda^{i-3}. \tag{28}$$

These expressions will be employed to calculate the strain rate $\dot{\epsilon}$ that will be used to evaluate and minimize the dissipation energy.

## III. POWER-LAW VISCOPLASTIC MATERIALS

### III.1. *General formulation*

To study the flow properties of composites using the models discussed above, we consider the matrix as a ductile, incompressible material described by the power-law (1). While the present analysis is carried out for a viscoplastic material, the results for power-law hardening plastic materials can be obtained in the same way when the strain rate quantities are identified as strain quantities.

Using the power law (1) and the von Mises flow rule (2), we obtain the multiaxial stress-strain rate relation

$$\boldsymbol{\sigma}' = \frac{2}{3}\frac{\sigma_0}{\dot{\epsilon}_0^m}\dot{\bar{\epsilon}}^{m-1}\dot{\boldsymbol{\epsilon}}. \tag{29}$$

As stated in Section II, we employ an energy approach to evaluate the macroscopic stress S from the dissipation energy (8). For incompressible materials, the local dissipation $\dot{w} = \boldsymbol{\sigma}\cdot\dot{\boldsymbol{\epsilon}}$ is given by

$$\dot{w} = \boldsymbol{\sigma}\cdot\dot{\boldsymbol{\epsilon}} = \left(\frac{2}{3}\right)^{(m+1)/2} \frac{\sigma_0}{\dot{\epsilon}_0^m} (\dot{\boldsymbol{\epsilon}}\cdot\dot{\boldsymbol{\epsilon}})^{(m+1)/2}. \tag{30}$$

Since $\dot{\boldsymbol{\epsilon}}\cdot\dot{\boldsymbol{\epsilon}} = \dot{\epsilon}^{ij}\dot{\epsilon}_{ij} = \dot{\epsilon}_i^j\dot{\epsilon}_j^i$, it is more convenient to employ the mixed components of the strain rate tensor $\dot{\epsilon}_i^j$ in nonorthogonal coordinate systems. The lengthy derivation from $(v_\alpha, v_\theta, v_\phi)$ to $\dot{\epsilon}_i^j$ is given in the Appendix. It is noted that the mixed components $\dot{\epsilon}_i^j$ are no longer symmetric.

It is also convenient to introduce $\dot{\boldsymbol{\epsilon}}^*$ such that the singular factor is separated from $\dot{\boldsymbol{\epsilon}}$,

$$\dot{\boldsymbol{\epsilon}} = \frac{D'}{3(1-\gamma)^3}\,\dot{\boldsymbol{\epsilon}}^*. \tag{31}$$

Then the macroscopic dissipation $\dot{W}$ can be written in the form

$$\dot{W} = \left(\frac{2}{3}\right)^{(m+1)/2} \left[\frac{D'}{3(1-\gamma)^3}\right]^{m+1} \frac{\sigma_0}{\dot{\epsilon}_0^m} \frac{1}{V}\int_V (\dot{\boldsymbol{\epsilon}}^*\cdot\dot{\boldsymbol{\epsilon}}^*)^{(m+1)/2}\, dV. \tag{32}$$

It can be easily seen from eqn (34) that $\dot{W}$ is homogeneous of degree $m+1$ in the macroscopic strain rate $\mathbf{D}$. Since a homogeneous function of $(m+1)$th degree has the property

$$\frac{\partial \dot{W}}{\partial \mathbf{D}}\cdot\mathbf{D} = (m+1)\dot{W}, \tag{33}$$

the equation for evaluating the macroscopic stress, (11), can be obtained directly by comparing (10) and (33).

For the axisymmetric deformations under consideration, substituting (32) into (11) gives the non-zero components of S in the Cartesian coordinate system as

$$\begin{aligned} S_{11} &= \frac{1}{2}\left(\frac{2}{3}\right)^{(m+1)/2} \frac{(D')^m}{[3(1-\gamma)^3]^{m+1}} \frac{\sigma_0}{\dot{\epsilon}_0^m} \frac{1}{V}\int_V (\dot{\boldsymbol{\epsilon}}^*\cdot\dot{\boldsymbol{\epsilon}}^*)^{(m+1)/2}\, dV, \\ S_{22} &= S_{11}, \\ S_{33} &= -2S_{11}. \end{aligned} \tag{34}$$

We note that for the axisymmetric deformations we have the simple relations $\bar{D} = 2D'/3$ and $\bar{S} = 3S_{11}$ where $\bar{D} = (2\mathbf{D}\cdot\mathbf{D}/3)^{1/2}$ and $\bar{S} = (3\mathbf{S}\cdot\mathbf{S}/2)^{1/2}$ are the effective macroscopic strain rate and effective macroscopic stress, respectively, which yields the effective stress–strain rate relation of the composite

$$\bar{S} = \frac{(\bar{D})^m}{[\sqrt{6}(1-\gamma)^3]^{m+1}} \frac{\sigma_0}{\dot{\epsilon}_0^m} \frac{1}{V}\int_V (\dot{\boldsymbol{\epsilon}}^*\cdot\dot{\boldsymbol{\epsilon}}^*)^{(m+1)/2}\, dV. \tag{35}$$

This equation can be rewritten in a more compact form by introducing the following notation

$$S_0 = \sigma_0 F(m,f) G(m,f,K), \tag{36}$$

with

$$F(m,f) = \frac{1}{(1-f^{1/3})^{3(m+1)}}, \tag{37}$$

$$G(m,f,K) = \frac{1}{V}\int_V \left(\frac{\dot{\epsilon}^* \cdot \dot{\epsilon}^*}{6}\right)^{(m+1)/2} dV, \tag{38}$$

where $f = \gamma^3$ is the volume fraction of the inclusion. Now the overall constitutive relation for the composite has the form of

$$\bar{S} = S_0 \left(\frac{\bar{D}}{\dot{\epsilon}_0}\right)^m. \tag{39}$$

The result given by eqn (39) indicates that the composite obeys a power-law relation with the same strain rate sensitivity as that of the matrix. The ratio of reference stresses $S_0/\sigma_0$ denotes the strength enhancement of the composite over the matrix. Eqns (36–38) show that this strength enhancement depends on the strain rate sensitivity of the matrix $m$, the particle volume fraction $f$, and the particle aspect ratio $K$ through a singular function $F$ and a regular integral function $G$. The issue now is to evaluate the integral $G(m,f,K)$ for various values of material parameters and unit cell geometries.

### III.2. *Numerical analysis for ellipsoidal inclusions*

In the general case of ellipsoidal inclusions and nonlinear matrices, the minimization of $\dot{W}$ and the integration of $G$ must be performed numerically. In both calculations, the central issue is to evaluate the integral

$$\frac{1}{V}\int_V (\dot{\epsilon}^* \cdot \dot{\epsilon}^*)^{(m+1)/2} dV. \tag{40}$$

Comparing eqn (32) to eqn (38) one can conclude that the minimization of $\dot{W}$ is equivalent to the minimization of $G$. Therefore, we directly minimize

$$G = G(\{c_{2i}\}, m, f, K) \tag{41}$$

with respect to $\{c_{2i}\}$. Then, the reference stress ratio is given by

$$\frac{S_0}{\sigma_0} = F(m,f) G_{min}(m,f,K). \tag{42}$$

In other words, the minimization of $\dot{W}$ and the evaluation of strength can be combined into one step and the volume integral (40) is calculated once for a given set of material parameters $(m,f,K)$.

The multidimensional minimization method adopted here is the downhill simplex method by NELDER and MEAD [1965]. This method simply moves downhill in a straightforward fashion. It is very robust since it makes almost no special assumptions about the function and requires only function evaluations, not derivatives. These features are important to the present analysis because $G$ is a function consisting of a double integral and thus not very smooth after the numerical quadrature.

Theoretically, one needs to consider a large number of terms in the series (28) to ensure a good quantitative accuracy. Fig. 2a shows the results obtained for various number of terms with positive and nonpositive powers; i.e., choosing a finite number of terms in the series (28) with $l \leq i \leq n$ ($l \leq 1$, $n > 1$). By setting $l = 1$ and $n > 1$ we consider only terms with positive powers in the stream function. For this case it can be seen from the figure that as $n$ is increased, the difference between adjacent curves diminishes, implying that the solution is converging. It can also be deduced from the figure that

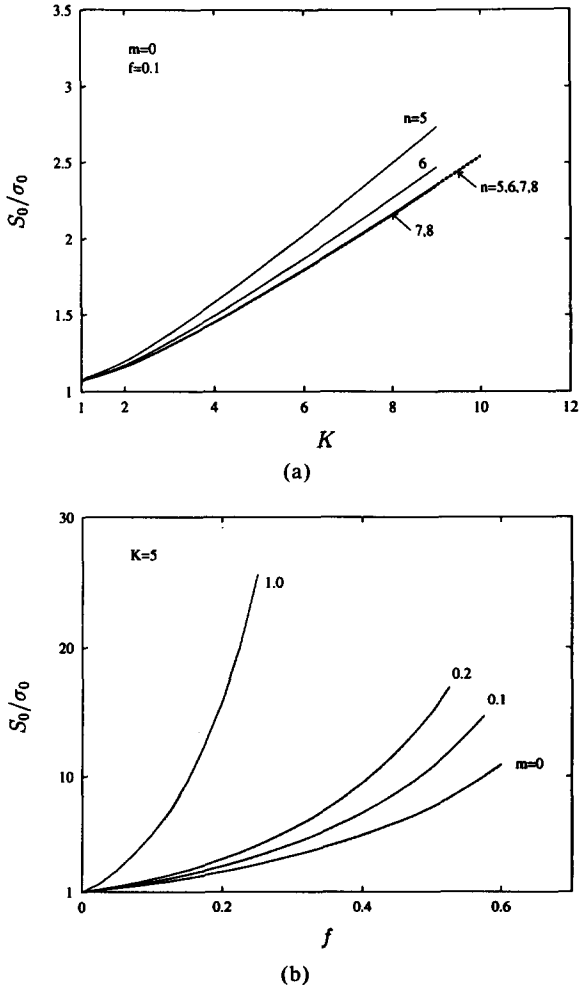


Fig. 2. The dependence of solutions on the number of terms in the series. (a) Solid lines: $l = 1$; dashed lines $l = -3$. (b) Solid lines $l = 1$, $n = 7$; dashed lines: $l = -3$, $n = 7$.

$n = 8$ gives a very good approximation since the error between the results of $n = 7$ and $n = 8$ is negligible. Next, we consider the effect of terms with negative powers in the stream function by setting $l = -3$ [i.e., including the terms $\lambda^{-5}, \lambda^{-4}, \ldots, \lambda^{-2}$ in (28)]. The results of this case is also shown in Fig. 2a as dashed curves. It is seen that the curves converge to the same solution as that without non-positive powers. In fact, the quantitative difference between the two cases of ($l = 1$, $n = 8$) and ($l = -3$, $n = 8$) is less than 1%.

Fig. 2b shows the effect of the matrix property on the composite strength. The particles are rigid ellipsoids of revolution with the aspect ratio $K = 5$. Higher strain rate sensitivity $m$ of the matrix results in higher strength of the composite, as expected. Shown in the figure are curves generated for the two cases ($l = 1$, $n = 7$) and ($l = -3$, $n = 7$). It is seen that adding terms with nonpositive powers does not yield appreciable improvement in the results. However, the use of terms with negative powers becomes more crucial for the case of an inclusion in an infinite media where the velocity field should decay rapidly. For example, BUDIANSKY *et al.* [1982] and DUVA [1984] used only terms with negative powers when dealing with the void-matrix and inclusion-matrix problems, respectively.

The effect of the particle aspect ratio $K$ on strength enhancement $S_0/\sigma_0$ is shown in Fig. 3 for both prolate and oblate ellipsoidal inclusions. The plastic flow in the composite is strongly dependent upon the particle shape in addition to the volume fraction. We define a shape index $K'$ as

$$K' = \begin{cases} K, & \text{for prolate inclusions,} \\ \dfrac{1}{K}, & \text{for oblate inclusions.} \end{cases} \tag{43}$$

so that for both prolate and oblate inclusions, a large $K'$ always indicates a shape far away from the sphere. As can be seen from Fig. 3, particles with large shape index $K'$ (i.e. whiskers or discs) exhibit much more reinforcement than that of spheres ($K' = 1$). The figure also shows that prolate particles (whiskers) are more effective than oblate

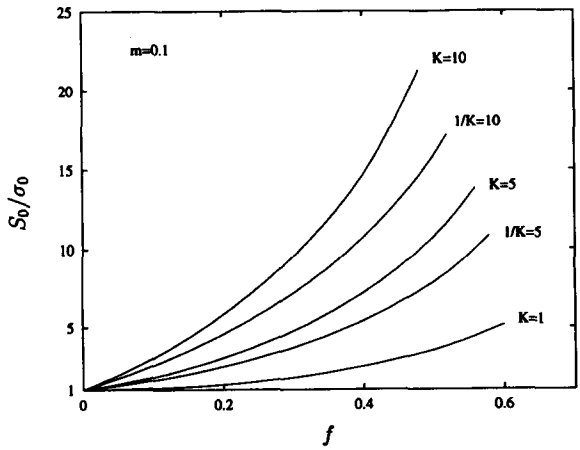


Fig. 3. Effect of particle shape on the flow strength of composites.

ones (discs) in strengthening the matrix. This is also observed by LEE and MEAR [1991] using a self-consistent approximation. The effect of particle shape is further illustrated in Fig. 4a and b for fixed levels of volume fraction. It is interesting to note that as the shape index $K'$ increases, the strength raito $S_0/\sigma_0$ tends to vary linearly with $K'$ for fixed volume fractions.

## IV. DISCUSSION

We have calculated the flow strength of composites with rigid particles and ductile matrix. The basic feature of the present results are consistent with that reported by EVANS *et al.* [1991], DUVA [1984], and BAO *et al.* [1991]. The work of DUVA [1984] considered a spherical inclusion in an infinite matrix and his model was constructed to be exact in the dilute limit for volume fractions up to 0.2. However, for $f > 0.2$ Duva's model underestimates the reinforcement. This point was further elaborated upon by

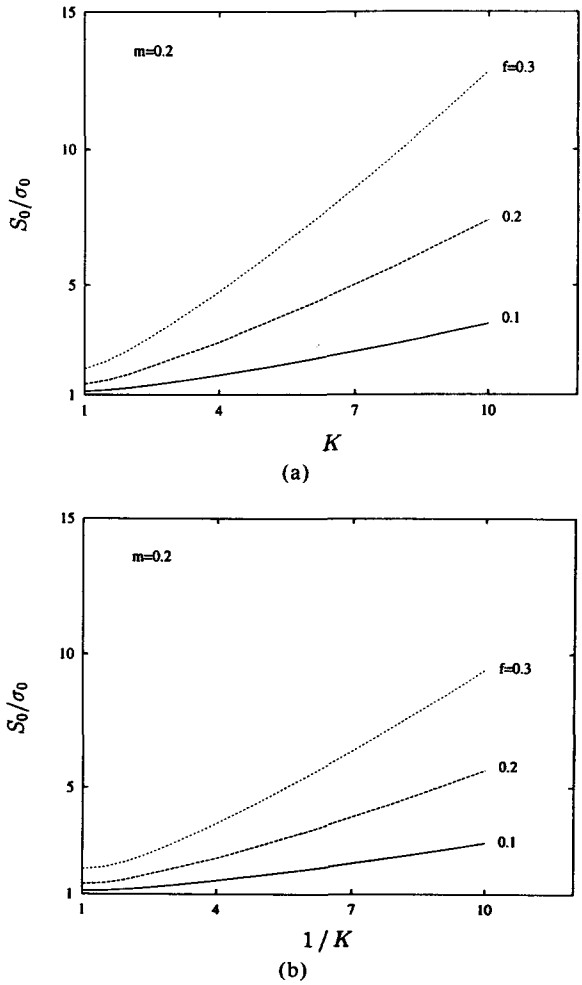


Fig. 4. Flow strength as a function of shape index. (a) Prolate particles. (b) Oblate particles.

EVANS *et al.* [1991] and BAO *et al.* [1991] who performed a finite element analysis. Their extensive numerical analysis yielded results similar to the present work.

Figs. 5 and 6 are plots of $S_0 - S^0$ normalized by $S^0 - \sigma_0$, versus $m$ for spherical and ellipsoidal inclusions, respectively, where $S^0$ is the strength of the composite when the matrix is perfectly plastic $m = 0$. For spherical inclusions (Fig. 5), the present model predicts results that are almost linear in $m$ and are close to those given by the finite element analysis of BAO *et al.* [1991]. The figure also shows that the result of Duva's model (DUVA [1984], recomputed by BAO *et al.* [1991]) given by the equation

$$\frac{S_0}{\sigma_0} = \frac{1}{(1-f)^{h(m)}}, \quad h(m) = 0.39(1-m) + \frac{5}{2}m, \tag{44}$$

overestimates the increase in the strength $S_0$ above $S^0$. Included in Fig. 6 are the same quantities for more heavily reinforced composites with aspect ratio ranging from 0.1 (a thin disc) to 10 (a long whisker). All results for $f = 0.1$, 0.2 and $K = 0.1$, 0.2, 5, 10 are located in a narrow regime indicated by two bounding curves in the figure, showing the little dependence on the details of the inclusion structure when aspect ratios are large.

As stated before, the model developed in this study for the viscoplastic matrix can be directly applied to power law strain hardening materials obeying the $J_2$-deformation theory of plasticity, due to the exact analogy between the structure of their constitutive equations. This allows us to compare the experimentally measured plastic properties of composites with the predictions based on the present model. Since our model is concerned with the behavior of the composite when the matrix becomes fully plastic with negligible elasticity, all experimental data have been converted to stress-plastic strain curves.

Fig. 7 shows the comparison between the model calculations and the measured tensile properties of an Al-SiC composite (YANG *et al.* [1991]) for three different volume fractions of the particulates, namely, 0.17, 0.30, and 0.48. The aspect ratio $K$ used in the calculation is taken to be 2 as reported in the experiment. The stress-plastic strain

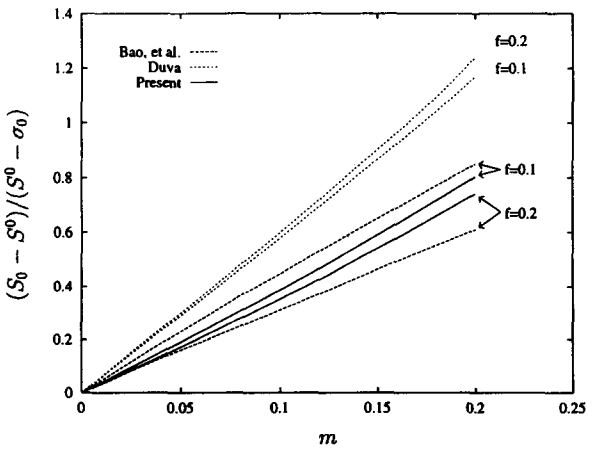


Fig. 5. Flow strength of composites with power-law hardening matrix over that with perfect-plastic matrix for spherical particles.

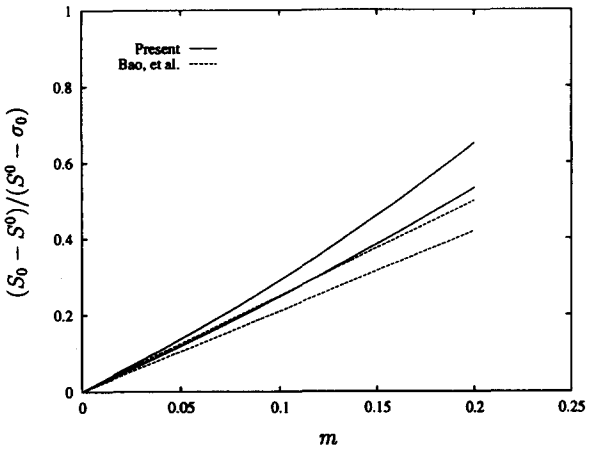


Fig. 6. Bounds for the flow strength of composites with power-law hardening matrix over that with perfect-plastic matrix for ellipsoidal particles with $f = 0.1$, 0.2 and $K = 0.1$, 0.2, 5, 10.

curve is fitted to the power law $\sigma = \sigma_0 \epsilon^m$, yielding $\sigma_0 = 93$ MPa and $m = 0.25$, which are then used in the calculation. It can be seen from the figure that the predictions by the current model agree very well with the experiments for volume fractions up to 0.3. Higher flow stresses are predicted for the highest particle volume fraction of 0.48. The somewhat lower strength displayed here by the experimental results is due to the misalignment of inclusions.

The predicted stress–plastic strain curves and experimental results (from CHRISTMAN *et al.* [1989b]) for a larger aspect ratio, $K = 5$, are plotted in Fig. 8. For this case the matrix parameters are given by $\sigma_0 = 0.57$ GPa and $m = 0.12$. The material is a Al-SiC whisker composite with a 13.2% SiC volume fraction. It is observed that the present model overestimates the stress–plastic strain response. Also given in Fig. 8 is a finite ele-

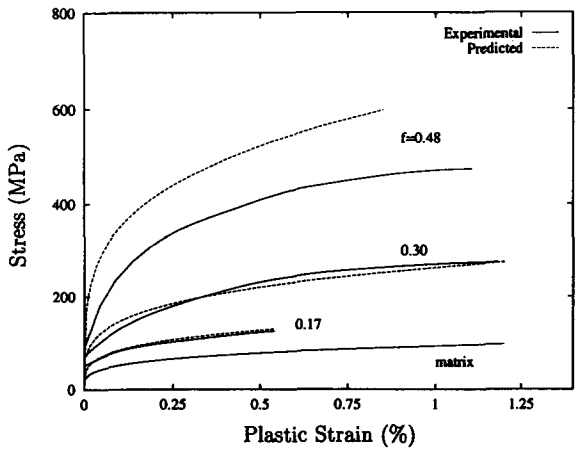


Fig. 7. Predicted stress-plastic strain curves compared to the experiments of YANG *et al.* [1991] on an Al-SiC composite.

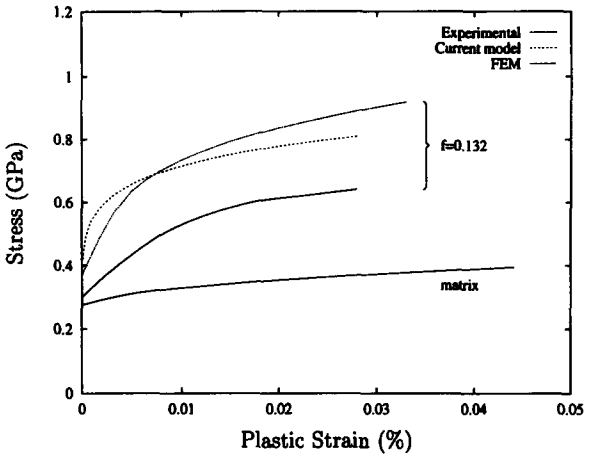


Fig. 8. Predicted stress-plastic strain curves for the composite with $K = 5$ compared to measured data and finite element analysis of CHRISTMAN *et al.* [1989b] on an Al-SiC whisker composite.

ment calculation by CHRISTMAN *et al.* [1989b], which employed an axisymmetric unit cell model where the aspect ratio of the unit cell was taken to be equal to the whisker aspect ratio and a sidewall constraint was imposed representing the periodic array. The features of the finite element model resemble the basic characters of the unit cell model proposed in this study and it is interesting to note that they give results close to each other.

The discrepancy between the predicted and measured results for the large aspect ratio can be attributed mainly to two factors. First, in the theoretical model the whiskers are perfectly aligned while misalignment of the whiskers from the tensile axis in real composites is commonly observed, which reduces the flow strength of composites. Second, the theoretical calculations are based on the assumption of uniform particle distribution, which is an idealized model. The clustering of reinforcement is common in real composites. Detailed finite element analysis (CHRISTMAN *et al.* [1989a]) has revealed that the nonuniform distribution of particles may drastically reduce the flow stress of the composite. This issue will be further addressed in a future article within a nonlocal continuum mechanics approach.

The model predictions for composites with a particle aspect ratio of 1 are qualitatively in good agreement with the experiments of NIEH and CHELLMAN [1984], but quantitatively lower, as shown in Fig. 9. However, it seems not proper to make a direct comparison because the material tested was reinforced by particles containing very sharp corners as discussed by CHRISTMAN *et al.* [1989a], which give rise to localized plastic strains that do not occur for smooth spherical particles in the model. Furthermore, effects of particle misalignment and clustering are minimal for an aspect ratio of 1, in contrast to large particle aspect ratios where the flow strength drops pronouncedly.

### IV.1. *An approximate model*

With all the results obtained analytically and numerically for both spherical and ellipsoidal inclusion, we are ready to propose an approximate model for the strength of the composite, $S_0$. The general form of $S_0$ is given by eqns (36–38). It consists of the reference stress of the matrix material multiplied by a factor representing the reinforcement

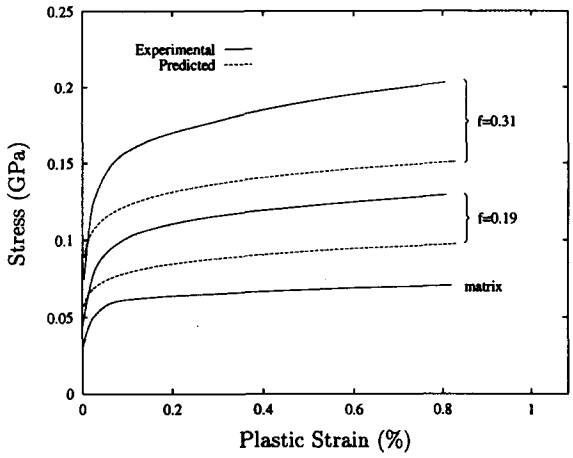


Fig. 9. Predicted stress-plastic strain curves for composites with spherical particles compared to the experimental results of NIEH and CHELLMAN [1984] on Al-SiC composites containing particles with sharp corners.

of the particles. This reinforcement factor has two parts. One is the function $F(m,f)$, which is singular and approaches infinity when $f \to 1$ representing the limiting case when the whole material becomes a rigid solid. This function comes naturally from the kinematic boundary conditions. Note that $F$ is not a function of $K$, which measures the inclusion shape. The other part of the reinforcement factor is the integral function $G(m,f,K)$, reflecting the volume averaging process. It is more complex than $F$ and needs a closer examination.

First, we isolate the shape effect aside by considering a spherical inclusion, i.e. the case of $K = 1$. Fig. 10a depicts $G$ versus $f$ for various values of $m$. It shows that $G$ decreases rapidly and approaches to zero as the volume fraction increases. In fact at $f = 1$, $G = 0$, which suggests that $G$ contains only one root. Further analysis reveals that $G$ may be represented in the form

$$(G)_{\text{sph}} = (1 - \gamma)^{(3/2)(m+1)} \bar{G}, \tag{45}$$

where the subscript "sph" indicates the quantity for spherical inclusions and $\bar{G}$ is a well behaved function of $\gamma$ (or $f$) with finite and non-zero values in the whole range of the volume fraction. Fig. 10b is a plot of $\bar{G}$ versus $\gamma$. For the typical values of $m \leq 0.2$ and $f \leq 0.2$, $\bar{G}$ can be represented by the approximate form

$$\bar{G} = 1 + a_1 f^{1/3} + a_2 f^{2/3} + a_3 f, \tag{46}$$

where $a_1, a_2, a_3$ are assumed to be linear in $m$. By fitting eqn (45) to the exact values of $G$, as obtained from the numerical evaluation of the integral (38) for various values of $m$, we obtain the approximate values

$$\begin{aligned} a_1 &= -1.34 - 1.56m, \\ a_2 &= -0.32 + 237m, \\ a_3 &= 1.11 - 0.53m. \end{aligned} \tag{47}$$

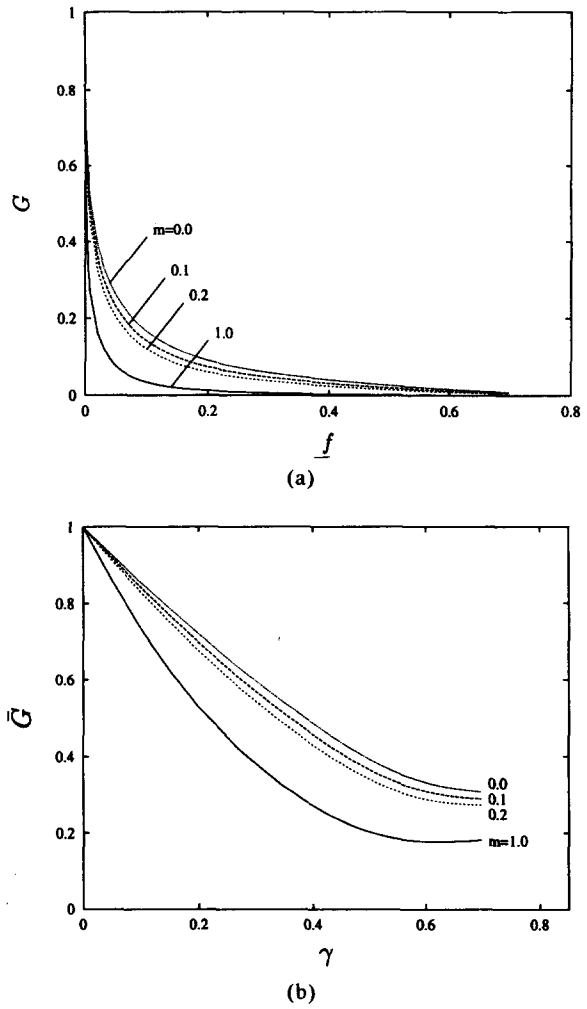


Fig. 10. Development of the approximate model for spherical particles. (a) Function $G$ with $K = 1$ versus volume fraction $f$. (b) Function $G$ with $K = 1$ versus $\gamma (= f^{1/3})$.

Therefore, for composites with power-law viscoplastic matrices reinforced by spherical inclusions, we have the approximate analytical expression

$$\left(\frac{S_0}{\sigma_0}\right)_{\text{sph}} = \frac{1 + a_1 f^{1/3} + a_2 f^{2/3} + a_3 f}{(1 - f^{1/3})^{(3/2)(m+1)}}, \quad m \leq 0.2, f \leq 0.2. \tag{48}$$

This hardening law for composites with spherical particles gives results that are very close to the exact values predicted by the integral relations (36–38) as shown in Fig. 11.

Next we extend the model given by eqn (48) to the general case of composites with ellipsoidal inclusions. We begin by noting that composites with ellipsoidal inclusions (either prolate or oblate) have higher flow strength than those with spherical particles as can be deduced from Fig. 4a and b. Thus, we propose that the reinforcement function $G$ for composites with ellipsoidal inclusions can be decomposed into two parts, one

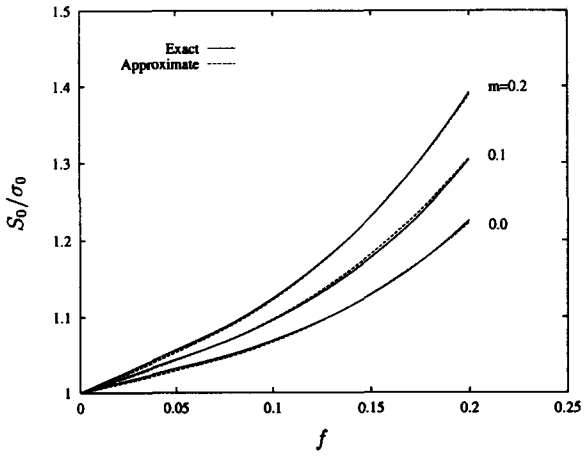


Fig. 11. Comparison of the proposed analytical expression for the flow strength of composites with spherical particles ($K = 1$) with the exact solution.

being the spherical reinforcement factor $G_{\text{sph}}$ and the second reflecting the increased reinforcement due to shape changes from sphere to ellipsoids. Thus, for general ellipsoidal inclusions, we propose the simple relation

$$G(m,f,K) = (1 + \alpha\beta f)G_{\text{sph}}, \tag{49}$$

where $\beta$ is a function measuring the influence of the aspect ratio $K$ and $\alpha$ is a general function of $m$. The factor $(1 + \alpha\beta f)$ reflects the shape effect and it should have the property that at $K = 1$, $\beta = 0$. (Of course, other forms can be used, but this turns out to be the simplest and to fit the data very well.)

For $m \leq 0.2$, $f \leq 0.2$ and $0.1 \leq K \leq 10$, within a single expression for both prolate and oblate inclusions, the following forms of $\alpha$ and $\beta$ give a simple yet accurate approximation to the numerical integrations:

$$\alpha = 1 + 2.6m,$$

$$\beta = -3.01 + 1.69K + 1.32\frac{1}{K}. \tag{50}$$

Then, eqn (49) along with (39) imply

$$\frac{S_0}{\sigma_0} = [1 + \beta f(1 + 2.6m)]\left(\frac{S_0}{\sigma_0}\right)_{\text{sph}}. \tag{51}$$

Results of the approximate models given above are compared to the exact values obtained from eqns (36–38) and are plotted in Fig. 12a and b. The model proposed by eqn (51) gives excellent results as can be deduced from these figures. Eqn (51) clearly shows the effect of the particle shape factor $\beta$ and the advantage of nonsphere particles in reinforcing the metal matrix over spherical particles.

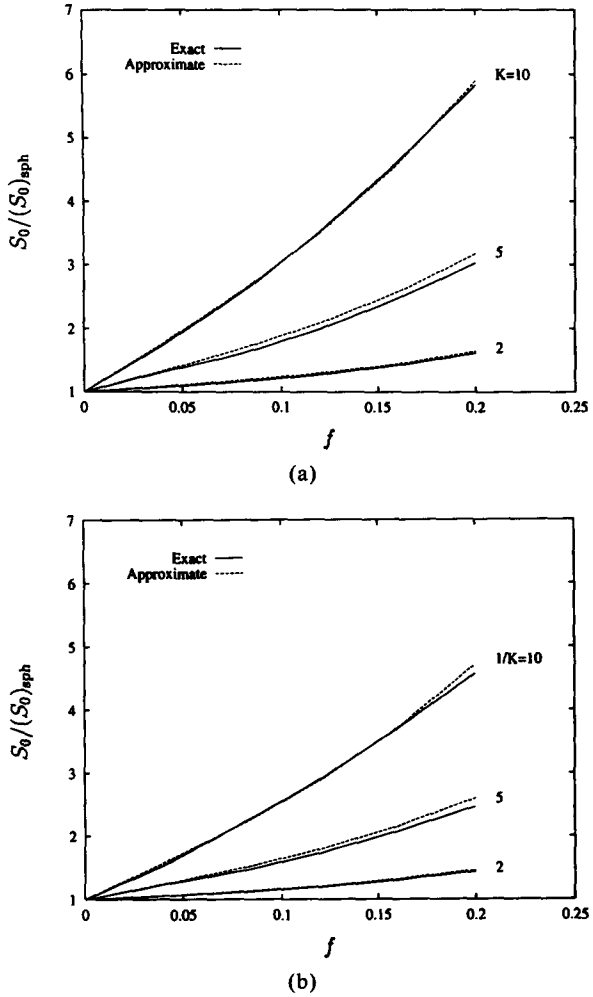


Fig. 12. Comparison between the exact solution and the proposed analytical expression for the flow strength of composites with nonspherical particles over that with spherical ones. Shown are curves for $m = 0.1$. (a) Prolate particles. (b) Oblate particles.

In summary, a continuum model for the flow strength of particulate-reinforced metal matrix composites has been rigorously developed. It consists of finite unit cells with a ductile matrix containing a single rigid inclusion in each cell. The analytical approach is based on an upper bound solution in which a kinematically admissible velocity field is assumed, and the total potential of the system is minimized. It is shown that this model has successfully captured basic features of the nonlinear plastic response of the composite and identified effects of particle shape and volume fraction on the overall flow properties of the composite. The results predicted by the current model compare very well with data found in the literature which are obtained experimentally or based on expensive finite element analyses. Furthermore, an explicit expression for the composite strength is proposed that accounts for various materials parameters, i.e. matrix properties, volume fraction parameter, and shape effects.

*Acknowledgement*—The support of the National Science Foundation under grant number MSS-9302327 is gratefully acknowledged.

## REFERENCES

1951 BISHOP, J.F.W., and HILL, R., "A Theory of the Plastic Distortion of a Polycrystalline Aggregate Under Combined Stresses," Phil. Mag., **42**, 414.
1965 HILL, R., "A Self-Consistent Mechanics of Composite Materials," J. Mech. Phys. Solids, **13**, 213.
1965 NELDER, J.A., and MEAD, R., "A Simplex Method for Function Minimization," Computer Journal, **7**, 308.
1969 MALVERN, L.E., Introduction to the Mechanics of a Continuum Medium, Prentice-Hall, Inc., Englewood Cliffs, NJ.
1971 MOON, P., and SPENCER, D.E., Field Theory Handbook, Springer, Berlin.
1973 MORI, T., and TANAKA, K., "Average Stress in the Matrix and Average Elastic Energy of Materials With Misfitting Inclusions," Acta Metall., **21**, 571.
1977 GURSON, A.L., "Continuum Theory of Ductile Rupture by Void Nucleation and Growth: Part I—Yield Criteria and Flow Rules for Porous Ductile Media," J. Engng. Mat. Tech., **99**, 2.
1980 BROWN, L.M., in HAASEN, P., GEROLD, V., and KOSTORZ, G., eds., Strength of Metals and Alloys, Pergamon Press, New York, p. 1151.
1982 BUDIANSKY, B., HUTCHINSON, J.W., and SLUTSKY, S., in HOPKINS, H.G., and SEWELL, M.J., eds., Mechanics of Solids, Pergamon Press, New York, p. 13.
1984 DUVA, J.M., "A Self-Consistent Analysis of the Stiffening Effect of Rigid Inclusions on a Power-Law Material," J. Engng. Mat. Tech., **106**, 317.
1984 DUVA, J.M., and HUTCHINSON, J.W., "Constitutive Potentials for Dilutely Voided Nonlinear Materials," Mech. Mater., **3**, 41.
1984 NIEH, T.G., and CHELLMAN, D.J., "Modulus Measurements in Discontinuous Reinforced Aluminum Composites," Scripta Metall., **18**, 925.
1984 WENG, G.J., "Some Elastic Properties of Reinforced Solids, with Special Reference to Isotropic Ones Containing Spherical Inclusions," Int. J. Eng. Sci., **22**, 845.
1989a CHRISTMAN, T., NEEDLEMAN, A., and SURESH, S., "An Experimental and Numerical Study of Deformation in Metal-Ceramic Composites," Acta Metall., **37**, 3029.
1989b CHRISTMAN, T., NEEDLEMAN, A., NUTT, S., and SURESH, S., "On Microstructural Evolution and Micromechanical Modelling of Deformation of a Whisker-Reinforced Metal-Matrix Composites," Mater. Sci. Engng., **107A**, 49.
1990 LEVY, A., and PAPAZIAN, J.M., "Tensile Properties of Short Fiber-Reinforced SiC/Al Composites: Part II. Finite-Element Analysis," Metall. Trans., **21A**, 411.
1990 PAPAZIAN, J.M., and ADLER, P.N., "Tensil Properties of Short Fiber-Reinforced SiC/Al Composites: Part I. Effects of Matrix Precipitates," Matell. Trans., **21A**, 401.
1990 TVERGAARD, V., "Analysis of Tensile Properties for a Whisker-Reinforced Metal Matrix Composite," Acta Metall. Mater., **38**, 185.
1990 ZHAO, Y.H., and WENG, G.J., "Theory of Plasticity for a Class of Inclusion and Fiber-Reinforced Composites," in WENG, G.J., TAYA, M., and ABÉ, H., eds., Micromechanics and Inhomogeneity, Springer-Verlag, New York, p. 599.
1991 BAO, G., HUTCHINSON, J.W., and MCMEEKING, R.M., "Particle Reinforcement of Ductile Matrices Against Plastic Flow and Creep," Acta Metall. Mater., **39**, 1871.
1991 EVANS, A.G., HUTCHINSON, J.W., and MCMEEKING, R.M., "Stress–Strain Behavior of Metal Matrix Composites With Discontinuous Reinforcements," Scripta Metall. Mater., **25**, 3.
1991 KAMAT, S.V., ROLLET, A.D., and HIRTH, J.P., "Plastic Deformation in Al-Alloy Matrix-Alumina Particulate Composites," Scripta Metal. Mater., **25**, 27.
1991 LEE, B.J., and MEAR, M.E., "Effect of Inclusion Shape on the Stiffness of Nonlinear Two-Phase Composites," J. Mech. Phys. Solids, **39**, 627.
1991 PONTE CASTANEDA, P., "The Effective Mechanical Properties of Nonlinear Isotropic Composites," J. Mech. Phys. Solids, **39**, 45.
1991 QIU, Y.P., and WENG, G.J., "The Influence of Inclusion Shape on the Overall Elasto-Plastic Behavior of a Two-Phase Isotropic Composites," Int. J. Solids Struct., **27**, 1537.
1991 VIEWPOINT SET, No. 15, Scripta Metall. Mater., **25**, 2.
1991 YANG, J., PICKARD, S.M., CADY, C., EVANS, A.G., and MEHRABIAN, R., "The Stress/Strain Behavior of Aluminum Matrix Composites With Discontinuous Reinforcements," Acta Metall. Mater., **39**, 1863.
1992 LEE, B.J., and MEAR, M.E., "Effective Properties of Power-Law Solids Containing Elliptical Inhomogeneities: Part I: Rigid Inclusions," Mech. Mater., **13**, 313.

1993 Li, G., and Ponte Castaneda, P., "Constitutive Models for Ductile Solids Reinforced by Rigid Spheroidal Inclusions," Mech. Mater., **15**, 279.

Department of Mechanical and Materials Engineering
Washington State University
Pullman, WA 99164-2920, USA

(*Received in final revised form* 10 *July* 1994)

## APPENDIX

### *Change of basis*

The covariant base vectors $(\mathbf{g}_1,\mathbf{g}_2,\mathbf{g}_3)$ in a curvilinear system $(x^1,x^2,x^3)$ may be defined by the transformation, from the rectangular Cartesian coordinates $(z^1,z^2,z^3)$ with unit base vectors $(\mathbf{i}_1,\mathbf{i}_2,\mathbf{i}_3)$, as

$$\mathbf{g}_s = \frac{\partial z^r}{\partial x^s}\,\mathbf{i}_r, \quad s,r = 1,2,3, \tag{A1}$$

where a repeated index implies summation. Similarly, we define the contravariant base vector $\mathbf{g}^r$ as

$$\mathbf{g}^r = \frac{\partial x^r}{\partial z^s}\,\mathbf{i}^s, \quad s,r = 1,2,3, \tag{A2}$$

where $\mathbf{i}^s = \mathbf{i}_s$ for Cartesian coordinates. For the prolate ellipsoidal system $(x^1,x^2,x^3) = (\alpha,\theta,\phi)$ as defined by eqn (12), we have

$$\begin{aligned}
\mathbf{g}_1 &= (\sinh\eta)\sin\theta\cos\phi\mathbf{i}_1 + (\sinh\eta)\sin\theta\sin\phi\mathbf{i}_2 + (\cosh\eta)\cos\theta\mathbf{i}_3,\\
\mathbf{g}_2 &= (\sinh\eta)\alpha\cos\theta\cos\phi\mathbf{i}_1 + (\sinh\eta)\alpha\cos\theta\sin\phi\mathbf{i}_2 - (\cosh\eta)\alpha\sin\theta\mathbf{i}_3,\\
\mathbf{g}_3 &= -(\sinh\eta)\alpha\sin\theta\sin\phi\mathbf{i}_1 + (\sinh\eta)\alpha\sin\theta\cos\phi\mathbf{i}_2,
\end{aligned} \tag{A3}$$

and

$$\begin{aligned}
\mathbf{g}^1 &= \frac{\sin\theta\cos\phi}{\sinh\eta}\,\mathbf{i}_1 + \frac{\sin\theta\sin\phi}{\sinh\eta}\,\mathbf{i}_2 + \frac{\cos\theta}{\cosh\eta}\,\mathbf{i}_3,\\
\mathbf{g}^2 &= \frac{\cos\theta\cos\phi}{(\sinh\eta)\alpha}\,\mathbf{i}_1 + \frac{\cos\theta\sin\phi}{(\sinh\eta)\alpha}\,\mathbf{i}_2 - \frac{\sin\theta}{(\cosh\eta)\alpha}\,\mathbf{i}_3,\\
\mathbf{g}^3 &= -\frac{\sin\phi}{(\sinh\eta)\alpha\sin\theta}\,\mathbf{i}_1 + \frac{\cos\phi}{(\sinh\eta)\alpha\sin\theta}\,\mathbf{i}_2.
\end{aligned} \tag{A4}$$

For the oblate ellipsoidal system defined by eqn (13), the base vectors are

$$\mathbf{g}_1 = (\cosh\eta)\sin\theta\cos\phi\mathbf{i}_1 + (\cosh\eta)\sin\theta\sin\phi\mathbf{i}_2 + (\sinh\eta)\cos\theta\mathbf{i}_3,$$

$$\mathbf{g}_2 = (\cosh\eta)\alpha\cos\theta\cos\phi\mathbf{i}_1 + (\cosh\eta)\alpha\cos\theta\sin\phi\mathbf{i}_2 - (\sinh\eta)\alpha\sin\theta\mathbf{i}_3, \tag{A5}$$

$$\mathbf{g}_3 = -(\cosh\eta)\alpha\sin\theta\sin\phi\mathbf{i}_1 + (\cosh\eta)\alpha\sin\theta\cos\phi\mathbf{i}_2$$

and

$$\mathbf{g}^1 = \frac{\sin\theta\cos\phi}{\cosh\eta}\mathbf{i}_1 + \frac{\sin\theta\sin\phi}{\cosh\eta}\mathbf{i}_2 + \frac{\cos\theta}{\sinh\eta}\mathbf{i}_3,$$

$$\mathbf{g}^2 = \frac{\cos\theta\cos\phi}{(\cosh\eta)\alpha}\mathbf{i}_1 + \frac{\cos\theta\sin\phi}{(\cosh\eta)\alpha}\mathbf{i}_2 - \frac{\sin\theta}{(\sinh\eta)\alpha}\mathbf{i}_3, \tag{A6}$$

$$\mathbf{g}^3 = -\frac{\sin\phi}{(\cosh\eta)\alpha\sin\theta}\mathbf{i}_1 + \frac{\cos\phi}{(\cosh\eta)\alpha\sin\theta}\mathbf{i}_2.$$

The transformation between the contravariant components of the same vector $\mathbf{u}$ in the two systems is obtained by first noting that

$$\mathbf{u} = u^s_{(x)}\mathbf{g}_s = u^r_{(z)}\mathbf{i}_r. \tag{A7}$$

Then using (A1) and defining

$$Q^r_s = \frac{\partial z^r}{\partial x^s}, \tag{A8}$$

we obtain

$$u^r_{(z)} = Q^r_s u^s_{(x)}. \tag{A9}$$

The matrix $Q^r_s$ for the transformation to the prolate ellipsoidal system turns out to be

$$[Q] = \begin{bmatrix} (\sinh\eta)\sin\theta\cos\phi & (\sinh\eta)\sin\theta\sin\phi & (\cosh\eta)\cos\theta \\ (\sinh\eta)\alpha\cos\theta\cos\phi & (\sinh\eta)\alpha\cos\theta\sin\phi & -(\cosh\eta)\alpha\sin\theta \\ -(\sinh\eta)\alpha\sin\theta\sin\phi & (\sinh\eta)\alpha\sin\theta\cos\phi & 0 \end{bmatrix}. \tag{A10}$$

For the oblate system the matrix is

$$[Q] = \begin{bmatrix} (\cosh\eta)\sin\theta\cos\phi & (\cosh\eta)\sin\theta\sin\phi & (\sinh\eta)\cos\theta \\ (\cosh\eta)\alpha\cos\theta\cos\phi & (\cosh\eta)\alpha\cos\theta\sin\phi & -(\sinh\eta)\alpha\sin\theta \\ -(\cosh\eta)\alpha\sin\theta\sin\phi & (\cosh\eta)\alpha\sin\theta\cos\phi & 0 \end{bmatrix}. \tag{A11}$$

It is noted that in the matrix notation (A9) has the form of

$$[u_{(z)}] = [Q]^T[u_{(x)}]. \tag{A12}$$

*The metric tensor*

The covariant components of the metric tensor $g_{mn}$ are defined as

$$g_{mn} = \mathbf{g}_m \cdot \mathbf{g}_n. \tag{A13}$$

For the prolate ellipsoidal system $g_{mn}$ are found to be

$$[g_{mn}] = \begin{bmatrix} \sinh^2\eta + \cos^2\theta & -\alpha \sin\theta\cos\theta & 0 \\ -\alpha \sin\theta\cos\theta & \alpha^2(\sinh^2\eta + \sin^2\theta) & 0 \\ 0 & 0 & \alpha^2 \sinh^2\eta \sin^2\theta \end{bmatrix} \tag{A14}$$

with its determinant $g$ being

$$g = |g_{mn}| = \alpha^4 \sinh^4\eta \cosh^2\eta \sin^2\theta. \tag{A15}$$

For the oblate ellipsoidal system,

$$[g_{mn}] = \begin{bmatrix} \sinh^2\eta + \sin^2\theta & \alpha \sin\theta\cos\theta & 0 \\ \alpha \sin\theta\cos\theta & \alpha^2(\sinh^2\eta + \cos^2\theta) & 0 \\ 0 & 0 & \alpha^2 \cosh^2\eta \sin^2\theta \end{bmatrix} \tag{A16}$$

with

$$g = \alpha^4 \sinh^2\eta \cosh^4\eta \sin^2\theta. \tag{A17}$$

The contravariant components of the metric tensor $g^{mn}$ are defined as

$$g^{mn} = \mathbf{g}^m \cdot \mathbf{g}^n. \tag{A18}$$

When $[g_{mn}]$ is given, the matrix $[g^{mn}]$ may also be calculated by

$$[g^{mn}] = [g_{mn}]^{-1}. \tag{A19}$$

For the prolate ellipsoidal system,

$$[g^{mn}] = \begin{bmatrix} \dfrac{\sinh^2\eta + \sin^2\theta}{\sinh^2\eta \cosh^2\eta} & \dfrac{\sin\theta\cos\theta}{\alpha \sinh^2\eta \cosh^2\eta} & 0 \\ \dfrac{\sin\theta\cos\theta}{\alpha \sinh^2\eta \cosh^2\eta} & \dfrac{\sinh^2\eta + \cos^2\theta}{\alpha^2 \sinh^2\eta \cosh^2\eta} & 0 \\ 0 & 0 & \dfrac{1}{\alpha^2 \sinh^2\eta \sin^2\theta} \end{bmatrix}. \tag{A20}$$

For the oblate ellipsoidal system,

$$[g^{mn}] = \begin{bmatrix} \dfrac{\sinh^2\eta + \cos^2\theta}{\sinh^2\eta\cosh^2\eta} & -\dfrac{\sin\theta\cos\theta}{\alpha\sinh^2\eta\cosh^2\eta} & 0 \\ -\dfrac{\sin\theta\cos\theta}{\alpha\sinh^2\eta\cosh^2\eta} & \dfrac{\sinh^2\eta + \sin^2\theta}{\alpha^2\sinh^2\eta\cosh^2\eta} & 0 \\ 0 & 0 & \dfrac{1}{\alpha^2\cosh^2\eta\sin^2\theta} \end{bmatrix}. \tag{A21}$$

These quantities are used to convert one form of tensor components, i.e. covariant, contravariant, mixed or physical components, to another. It is pointed out that both ellipsoidal systems are non-orthogonal.

*Covariant derivatives; Christoffel symbols*

The derivative of an arbitrary vector $\mathbf{u} = u_m\mathbf{g}^m$ in a curvilinear coordinate system is given by

$$\frac{\partial\mathbf{u}}{\partial x^n} = u_{m|n}\mathbf{g}^m. \tag{A22}$$

The quantities $u_{m|n}$ are the covariant derivatives defined as

$$u_{m|n} = u_{m,n} - \Gamma^s_{mn}u_s, \tag{A23}$$

where

$$\Gamma^s_{mn} = \frac{\partial^2 z^p}{\partial x^m\partial x^n}\frac{\partial x^s}{\partial z^p} \tag{A24}$$

are Christoffel symbols of the second kind (MALVERN [1969]).

It can be shown that the non-zero quantities of $\Gamma^m_{sn}$ for the prolate ellipsoidal coordinates are

$$\begin{aligned} \Gamma^1_{22} &= -\alpha \\ \Gamma^2_{12} &= \Gamma^2_{21} = \frac{1}{\alpha} \\ \Gamma^1_{33} &= -\alpha\sin^2\theta \\ \Gamma^2_{33} &= -\sin\theta\cos\theta, \end{aligned} \tag{A25}$$

and for the oblate ellipsoidal system,

$$\begin{aligned} \Gamma^1_{22} &= \alpha \\ \Gamma^2_{12} = \Gamma^2_{21} &= -\frac{1}{\alpha} \\ \Gamma^1_{33} &= -\alpha \sin^2 \theta \\ \Gamma^2_{33} &= -\sin \theta \cos \theta. \end{aligned} \tag{A26}$$

*Mixed components of the strain rate tensor*

The procedure deriving the mixed components of the strain rate tensor $\dot{\epsilon}^m_n$ from the physical components of the velocity $(v_\alpha, v_\theta, v_\phi)$ includes calculating the contravariant components of the velocity $v^m$, the covariant components of the velocity $v_m$, the covariant components of the strain rate $\dot{\epsilon}_{mn}$, and finally the mixed components $\dot{\epsilon}^m_n$.

First we introduce the following functions that will be used in the representations of some results:

$$\begin{aligned} F_1(\lambda) &= \sum_{k=-\infty}^{\infty} B_k \lambda^{k-2}, \\ F_2(\lambda) &= \sum_{k=-\infty}^{\infty} k B_k \lambda^{k-2}, \\ F_3(\lambda) &= \sum_{k=-\infty}^{\infty} (k-2) B_k \lambda^{k-3}, \\ F_4(\lambda) &= \sum_{k=-\infty}^{\infty} k(k-2) B_k \lambda^{k-3}, \\ F_5(\lambda) &= \sum_{k=-\infty}^{\infty} (k-1) B_k \lambda^{k-2}, \\ F_6(\lambda) &= \sum_{k=-\infty}^{\infty} k(k-1) B_k \lambda^{k-2}, \end{aligned} \tag{A27}$$

where $B_k$ and $\lambda$ are defined by eqn (27).

Since $(v_\alpha, v_\theta, v_\phi)$ in eqn (28) are the physical components of velocity parallel to $\mathbf{g}_m$, the contravariant components are simply

$$\begin{aligned} v^1 &= \frac{v_\alpha}{\sqrt{g_{11}}}, \\ v^2 &= \frac{v_\theta}{\sqrt{g_{22}}}, \\ v^3 &= \frac{v_\phi}{\sqrt{g_{33}}}. \end{aligned} \tag{A28}$$

The covariant components of velocity $v_m$ are related to the contravariant components $v^n$ by the metric tensor $g_{mn}$ as

$$v_m = g_{mn} v^n. \tag{A29}$$

Then eqn (28) along with (A28) and (A29) yield, for the prolate ellipsoidal system,

$$\begin{aligned} v_1 &= -\tfrac{1}{2}\alpha_2(\sinh^2\eta + \cos^2\theta)(1 + 3\cos 2\theta)F_1(\lambda) - \tfrac{1}{4}\alpha_2 \sin^2 2\theta F_2(\lambda), \\ v_2 &= \tfrac{1}{4}\alpha_2^2 \sin 2\theta(1 + 3\cos 2\theta)\lambda F_1(\lambda) + \tfrac{1}{2}\alpha_2^2(\sinh^2 + \sin^2\theta)\sin 2\theta\lambda F_2(\lambda), \\ v_3 &= 0, \end{aligned} \tag{A30}$$

and for the oblate ellipsoidal system,

$$\begin{aligned} v_1 &= -\tfrac{1}{2}\alpha_2(\sinh^2\eta + \sin^2\theta)(1 + 3\cos 2\theta)F_1(\lambda) + \tfrac{1}{4}\alpha_2 \sin^2 2\theta F_2(\lambda), \\ v_2 &= -\tfrac{1}{4}\alpha_2^2 \sin 2\theta(1 + 3\cos 2\theta)\lambda F_1(\lambda) + \tfrac{1}{2}\alpha_2^2(\sinh^2\eta + \cos^2\theta)\sin 2\theta\lambda F_2(\lambda), \\ v_3 &= 0. \end{aligned} \tag{A31}$$

The strain rate tensor is calculated by eqn (3), which may be written in the index notation as

$$\dot{\epsilon}_{mn} = \tfrac{1}{2}(v_{m|n} + v_{n|m}). \tag{A32}$$

Using (A22) through (A25), we find that the non-zero components of $\dot{\epsilon}_{mn}$ are

$$\begin{aligned} \dot{\epsilon}_{11} &= -\tfrac{1}{2}(\sinh^2\eta + \cos^2\theta)(1 + 3\cos 2\theta)F_3(\lambda) - \tfrac{1}{4}\sin^2 2\theta F_4(\lambda), \\ \dot{\epsilon}_{22} &= \alpha_2\lambda v_1 - \tfrac{1}{2}\alpha_2^2(3 - \cos 2\theta + 6\cos^2 2\theta)\lambda F_1(\lambda) \\ &\quad \times \tfrac{1}{2}\alpha_2^2[\sin^2 2\theta + 2(\sinh^2\eta + \sin^2\theta)\cos 2\theta]\lambda F_2(\lambda), \\ \dot{\epsilon}_{33} &= \alpha_2 \sin^2\theta\lambda v_1 + \sin\theta\cos\theta v_2, \\ \dot{\epsilon}_{12} &= \tfrac{1}{4}\alpha_2 \sin 2\theta[1 + 3\cos\theta + 6(\sinh^2\eta + \cos^2\theta)]F_1(\lambda) \\ &\quad - \tfrac{1}{4}\alpha_2 \sin 4\theta F_2(\lambda) + \tfrac{1}{8}\alpha_2 \sin 2\theta(1 + 3\cos\theta)F_5(\lambda) \\ &\quad + \tfrac{1}{4}\alpha_2 \sin 2\theta(\sinh^2\eta + \sin^2\theta)F_6(\lambda) - \frac{v_2}{\alpha_2\lambda}, \end{aligned} \tag{A33}$$

for the prolate ellipsoidal system and

$$\dot{\epsilon}_{11} = -\tfrac{1}{2}(\sinh^2\eta + \sin^2\theta)(1 + 3\cos 2\theta)F_3(\lambda) + \tfrac{1}{4}\sin^2 2\theta F_4(\lambda),$$

$$\dot{\epsilon}_{22} = \alpha_2\lambda v_1 + \tfrac{1}{2}\alpha_2^2(3 - \cos 2\theta + 6\cos^2 2\theta)\lambda F_1(\lambda)$$

$$\times \tfrac{1}{2}\alpha_2^2[-\sin^2 2\theta + 2(\sinh^2\eta + \cos^2\theta)\cos 2\theta]\lambda F_2(\lambda),$$

$$\dot{\epsilon}_{33} = \alpha_2 \sin^2\theta\lambda v_1 + \sin\theta\cos\theta v_2, \tag{A34}$$

$$\dot{\epsilon}_{12} = -\tfrac{1}{4}\alpha_2 \sin 2\theta[1 + 3\cos\theta - 6(\sinh^2\eta + \sin^2\theta)]F_1(\lambda)$$

$$+ \tfrac{1}{4}\alpha_2 \sin 4\theta F_2(\lambda) - \tfrac{1}{8}\alpha_2 \sin 2\theta(1 + 3\cos\theta)F_5(\lambda)$$

$$+ \tfrac{1}{4}\alpha_2 \sin 2\theta(\sinh^2\eta + \cos^2\theta)F_6(\lambda) - \frac{v_2}{\alpha_2\lambda},$$

for the oblate ellipsoidal system.

Finally, the mixed components $\dot{\epsilon}_n^m$ are obtained by

$$\dot{\epsilon}_n^m = g^{ms}\dot{\epsilon}_{sn}, \tag{A35}$$

where $g^{ms}$ are given by (A20) or (A21) for the prolate or oblate ellipsoidal system, respectively.